Commun. Comput. Phys.
doi: 10.4208/cicp.080115.010515s

Vol. **18**, No. 4, pp. 1095-1121
October 2015

Modelling Rarefied Hypersonic Reactive Flows Using the Direct Simulation Monte Carlo Method

Ming-Chung Lo[1], Cheng-Chin Su[1], Jong-Shinn Wu[1,*] and Kun-Chang Tseng[2]

[1] *Department of Mechanical Engineering, National Chiao Tung University, 1001 Ta-Hsueh Road, Hsinchu 30010, Taiwan.*
[2] *National Space Organisation, National Applied Research Laboratories, Hsinchu 30010, Taiwan.*

Received 8 January 2015; Accepted (in revised version) 1 May 2015

Abstract. This paper presents the implementation, validation and application of TCE (total collision energy) model for simulating hypersonic reactive flows in a parallel direct simulation Monte Carlo code, named PDSC^{++}, using an unstructured grid. A series of benchmarking test cases, which include reproduction of theoretical rate constants in a single cell, 2D hypersonic flow past a cylinder and 2D-axisymmetric hypersonic flow past a sphere, were performed to validate the implementation. Finally, detailed aerothermodynamics of the flown reentry Apollo 6 Command Module at 105 km is simulated to demonstrate the powerful capability of the PDSC^{++} in treating realistic hypersonic reactive flow at high altitude.

AMS subject classifications: 76P05

Key words: DSMC, chemistry, non-equilibrium, TCE (total collision energy), hypersonic.

1 Introduction

Hypersonic aerothermodynamics (ATD) has become an increasingly important research topics because of increasing suborbital or orbital space activities worldwide (25 km and beyond). The detailed understanding of hypersonic ATD, such as catalytic reaction and oxidation of thermal protection layer, real-gas effects on shock-boundary layer interactions, blackout and real-gas effects, is especially important for those reentry space vehicles with high-enthalpy flow fields due to very high speed of the space vehicles. Even though there have been many ground wind tunnel experiments, e.g., HEG [1], F4 [2] and

*Corresponding author. *Email addresses:* mingchungluo@gmail.com (M.-C. Lo), ccs1982.me95g@gmail.com (C.-C. Su), chongsin@faculty.nctu.edu.tw (J.-S. Wu), kctseng@nspo.narl.org.tw (K.-C. Tseng)

 ©2015 Global-Science Press

https://doi.org/10.4208/cicp.080115.010515s Published online by Cambridge University Press

LENS [3] and relatively limited flight experiments, e.g., SHEFEX [4], it is well known that our understanding of hypersonic ATD, such as pitching moment anomaly and heat flux over dimensioning, is not enough for optimizing the design of reentry vehicles in an efficient way. Recently, some more thorough reentry flight experiments, e.g., EXPERT [5], are now under planning to obtain more detailed ATD data for reentry space vehicles using advanced in-situ measurement techniques. In addition to the aforementioned expensive ground tests and very expensive flight experiments, numerical modeling is considered to be the most attractive and affordable alternative in understanding these complex hypersonic ATD in detail, which would lead to a better design of the space vehicles. In this paper, we aim at implementing and validating chemical reaction module into a previously developed parallel direct simulation Monte Carlo (DSMC) code, named PDSC^{++} [6–8], that can used for general rarefied hypersonic flow simulation. At the end, we will demonstrate its capability in simulating a challenging 3D hypersonic Apollo Command Module reentry flow at an altitude of 105 km.

DSMC [9] is a particle-based simulation method, which employs fundamental collision kinetics and was shown to be equivalent to solving the Boltzmann equation when the number of simulation particles is large [10]. It has become a standard simulation method in either rarefied or thermal non-equilibrium gas dynamics. The computational cost of DSMC is generally high, especially when the flow is in the transitional and near-continuum regime. Fortunately, DSMC is a highly localized numerical scheme, which is especially suitable for parallel computing through domain decomposition, because binary collision occurs in a limited space (e.g., cell). In the community, there are several legacy DSMC codes which are parallelized using message passing interface (MPI). These may include DAC [11], MONACO [12], SMILE [13] and PDSC^{++}. For properly modeling hypersonic reactive flow under rarefied environment, efficient and accurate treatment of various kinds of chemical reactions in microscopic state is necessary and is described next.

For modeling chemical reactions in a rarefied hypersonic flow using DSMC, some special techniques are necessary. Among these, the total collision energy model (TCE) [9] is the most popular one, which converts the macroscopic Arrhenius rate equations to microscopic reaction cross sections at the microscopic level. It was used to calculate the reaction probabilities for dissociation and exchange reactions. In addition, a three-body collision model proposed by Boyd [14] was found to treat the recombination reaction reasonably well. The Larsen-Borgnakke model [15] was employed to handle the energy exchange between translational, rotational, and vibrational modes. In this paper, these models are used to model the chemical reaction within the framework of the PDSC^{++}, which is described in later section.

In the study, the implementation of chemical reaction module in PDSC^{++} is described in detail and validated by several benchmark problems. Finally, challenging hypersonic reactive flow past the Apollo Command Module was simulated to demonstrate the powerful capability of the PDSC^{++} in treating realistic hypersonic flows.

https://doi.org/10.4208/cicp.080115.010515s Published online by Cambridge University Press

2 Numerical method

2.1 Standard DSMC method

The details of the DSMC method can be found in Bird [9]. One of the basic assumptions of the DSMC method is the decoupling of the movement and collision of particles, should the time step size be much smaller than the mean collision time. Briefly speaking, the DSMC method includes the procedures such as initialization, particle movement, indexing, particle collision, and sampling. For initialization, the velocities of particles are generally sampled from an equilibrium Maxwell-Boltzmann distribution and the spatial positions of the particles are randomly distributed in each cell. For particle movement, all particles move according to their current phase-space states (3 positions and 3 velocities). The particles are relocated to their destination either through free flight or interaction with various types of solid wall (e.g., diffusive, specular, absorptive). Particles are removed when their destinations lie outside the computational domain. For indexing, all particles are indexed with their resident cells to facilitate the efficient selection of particles during the collision phase. For particle collision, two particles in each cell are randomly selected and they are decided probabilistically whether collision occurs. The post-collision velocities are calculated according to the type of collision, such as elastic collision, translational-rotational energy transfer, translational-vibrational energy transfer, and reactive energy transfer. Prior to the selection of collision pairs in each cell during each time step, it is necessary that the maximal number of collision pairs be decided (e.g., No Time Counter, NTC [9]). For sampling, the post-collision velocities are sampled (or accumulated) in order to calculate the macroscopic flow properties. With the exception of initialization, all of these procedures are repeated until the sample size is large enough with an acceptable statistical uncertainty.

2.2 Parallel Direct Simulation Monte Carlo Code

The PDSC^{++} used in this study has several major features, which include: (a) unstructured grid for better treatment of the flow with complex geometry [6], (b) parallel computing with domain re-decomposition (RDR) technique to efficiently maintain an approximate load balance [16], (c) variable time-step (VTS) scheme [7,17] and transient adaptive sub-cell (TAS) scheme [8,18] for enhancing collision quality with greatly reduced number of simulation particles without losing solution accuracy.

2.3 Total Collision Energy (TCE) Model

Most gas-phase chemical reactions can be treated as serial collision processes in DSMC. The basic chemical reactions in DSMC are classified into dissociation, exchange and recombination. In the TCE model, the macroscopic Arrhenius rate equations are converted to the reaction probability at the microscopic level [9]. In the current study, we used the total collision energy (TCE) model for handling dissociation and exchange reactions.

https://doi.org/10.4208/cicp.080115.010515s Published online by Cambridge University Press

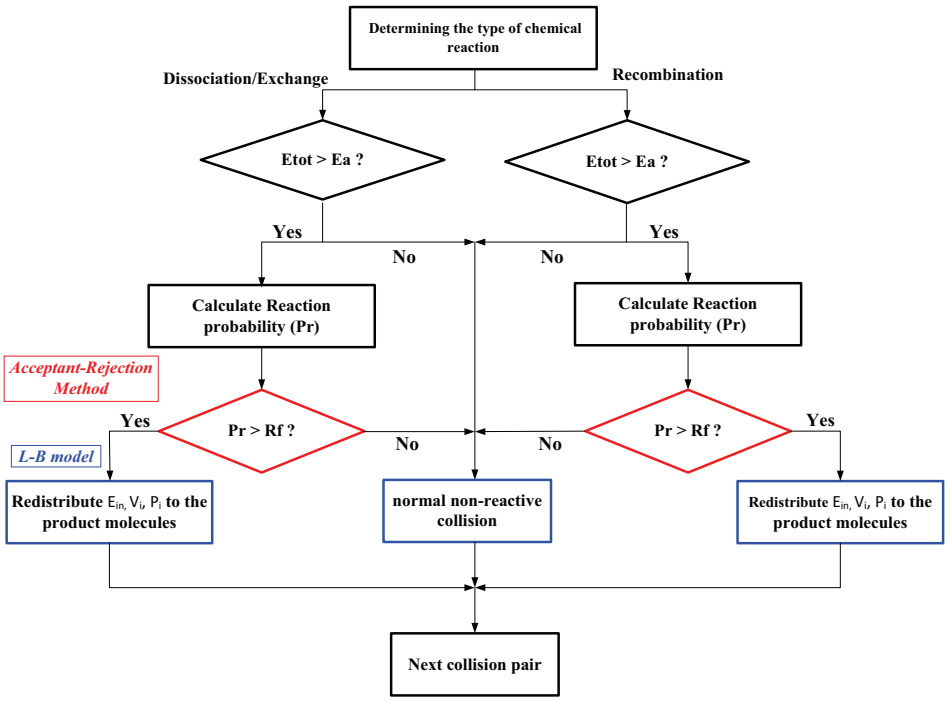


Figure 1: The flow chart of treatment of chemical reactions in PDSC^{++}.

Besides, an extended TCE model proposed by Boyd is used to treat the three-body recombination [14]. Details of the implementation are described next.

The flow chart of chemical models implemented in PDSC^{++} is illustrated in Fig. 1. The procedures include: (a) Determining which type of chemical reaction by the randomly selected collision pair. (b) Calculating the reaction probability of the specific chemical reaction if the total energy is greater than the activation energy of the reaction type. If not, then normal non-reactive collision is processed as usual. (c) Using acceptant-rejection method [9] to determine whether the chemical reaction occurs or not. If the chemical reaction occurs, then redistribute internal energies, velocities and positions for product particles using the Larsen-Borgnakke model for energy re-distribution among various degrees of freedom. If not, the normal non-reactive collision is processed. (d) Return to (a) for handling the next collision.

Details of the theoretical background of the various kinds of chemical reactions treated in PDSC^{++} are described next.

2.4 Dissociation reaction

A typical bimolecular reaction can be written as

$$A+B\rightarrow C+D, \tag{2.1}$$

https://doi.org/10.4208/cicp.080115.010515s Published online by Cambridge University Press

where A, B, C, D, respectively, represent different molecule, which can be either molecule or atom. The rate equation for the change of concentration of species A can be written

$$-\frac{dn_A}{dt}=k_f(T)n_An_B-k_r(T)n_Cn_D, \tag{2.2}$$

where k_f and k_r are the forward and reversed rate constants, respectively, which can be expressed in the following Arrhenius equation form as a function of temperature.

$$k_f(T)=aT^b\exp\left(-\frac{E_a}{kT}\right), \tag{2.3}$$

where a, b are constants. E_a and k are the activation energy and Boltzmann constant, respectively. The formulation is essentially macroscopic and these values are usually obtained by curve-fitting from the experimental data.

From classical kinetic theory, the production rate of the forward reaction can be written as [19]

$$k_fn_An_B=n_A\nu_{AB}\int_{\frac{E_c}{kT}}^{\infty}f\left(\frac{E_c}{kT}\right)\mathrm{P}_r\left(\frac{E_c}{kT}\right)d\left(\frac{E_c}{kT}\right), \tag{2.4}$$

where E_c is the total energy of the collision pairs and υ_{AB} is the collision frequency of molecule A with molecule B in an equilibrium gas, which may be expressed as

$$\nu_{AB}=\frac{n_B\overline{\sigma_Tc_r}}{\alpha}\qquad \alpha=1\ \text{ for }\ A\neq B,\quad \alpha=2\ \text{ for }\ A=B, \tag{2.5}$$

where n_B and α are the number density of B molecule and the symmetric factor, respectively. In addition, σ_T is the total collision cross section and c_r is the relative velocity of collision pair. Thus, $\overline{\sigma_Tc_r}$ is the average volume that one A-B particle pair sweeps per unit time, which can be further written as

$$\overline{\sigma_Tc_r}=\frac{2\sigma_{ref}}{\sqrt{\pi}}\left[(2-\omega)T_{ref}\right]^{\gamma}T(2-\gamma)\left(\frac{2k}{m_r}\right)T^{1/2-\gamma},\qquad \omega=\gamma+1/2, \tag{2.6}$$

where σ_{ref}, T_{ref} and m_r are the reference cross section, temperature and reduced mass, respectively. Note that ω is the viscosity-temperature exponent for $\mu\propto T^{\omega}$. By substituting Eq. (2.5) and Eq. (2.6) into Eq. (2.4), the dissociation probability can be obtained as

$$\mathrm{P}_r\left(\frac{E_c}{kT}\right)=\frac{\sigma_R}{\sigma_T}=\frac{\alpha\pi^{1/2}a{T_{ref}}^b}{2\sigma_{ref}(kT_{ref})^{b-1+\omega_{AB}}}\frac{\Gamma(\overline{\xi}+5/2-\omega_{AB})}{\Gamma(\overline{\xi}+b+3/2)}\left(\frac{m_r}{2kT_{ref}}\right)^{1/2}\frac{(E_c-E_a)^{b+\overline{\xi}+1/2}}{{E_c}^{\overline{\xi}+3/2-\omega_{AB}}}, \tag{2.7}$$

where $\overline{\xi}=(\xi_A+\xi_B)/2$ is the average number of internal degrees of freedom that contribute to the total collision energy. Thus, Eq. (2.7) is the dissociation probability that we use for the current PDSC^{++} code. Accordingly, the rate constant can be calculated as follows:

$$k_f=\frac{\overline{\sigma_Tc_r}}{\alpha}\int_{\frac{E_c}{kT}}^{\infty}f\left(\frac{E_c}{kT}\right)\mathrm{P}_r\left(\frac{E_c}{kT}\right)d\left(\frac{E_c}{kT}\right)=\frac{\overline{\sigma_Tc_r}}{\alpha}\overline{\mathrm{P}_r}. \tag{2.8}$$

https://doi.org/10.4208/cicp.080115.010515s Published online by Cambridge University Press

2.5 Recombination reaction

In the DSMC method, binary collisions are naturally assumed. Thus, it represents a challenge to simulate three-body recombination reactions, which are considered important in high-altitude air chemistry. In Vincenti and Kruger [20], it is stated that, for the recombination reaction, for example, between two nitrogen atoms and any third body M,

$$N+N+M\rightarrow N_2+M. \tag{2.9}$$

The rate of formation of N_2 is governed by

$$\frac{dn_{N_2}}{dt}=(k_b n_N n_N)n_M, \tag{2.10}$$

where n_N and n_M are the number densities of nitrogen atom and the third body M, respectively. Note k_b is the backward rate coefficient, which can be written as $k_b=k_f/K_c=(a_f/a_c)T^{b_f-b_c}$, where a_f and b_f are the constants for forward reaction, a_c and b_c are the constants for equilibrium reaction and K_c is the equilibrium constant. The expression in the parenthesis in Eq. (2.10) indicates that, in the new recombination model for the DSMC method, the reaction is first treated as a binary collision between two N atoms and followed by another binary collision. This allows the derivation of a recombination probability in the same way as for a dissociating reaction in the previous section. The correct reaction probability must then be multiplied by the number density of the third body n_m. The third body (M) is chosen randomly from those particles that exist in the collision cell, which can be any species. Thus, the number density of the third body is the total number density. The details of the derivation of the theoretical reaction probability and rate constants can be found in [14, 19]. They are only described briefly as follows:

$$\frac{dn_{N_2}}{dt}=(k_b n_N n_N)n_M=\left(\overline{\mathrm{P}_{r,b}}\cdot Z_{N,N}\right)\cdot n_M=\overline{\mathrm{P}_{r,new}}\cdot Z_{N,N}, \tag{2.11}$$

where $\overline{\mathrm{P}_{r,new}}=\overline{\mathrm{P}_{r,b}}\cdot n_M$, $\overline{\mathrm{P}_{r,b}}$ is the probability of binary collision between two atoms, $\overline{\mathrm{P}_{r,new}}$ is the new probability of the recombination reaction and $Z_{N,N}$ is the collision rate between nitrogen atoms. From Eq. (2.11), the rate constant can be obtained as follows:

$$(k_b n_N n_N)n_M=\overline{\mathrm{P}_{r,new}}\cdot Z_{N,N}=\overline{\mathrm{P}_{r,new}}\cdot\frac{n_N\cdot n_N\cdot\overline{\sigma g}}{\alpha}, \tag{2.12}$$

where α is defined similar to that in Eq. (2.5).

The form of the binary recombination probability is chosen as follows:

$$\overline{\mathrm{P}_{r,b}}=\left(\frac{1}{Z_r}\right)E_c{}^{\chi}, \tag{2.13}$$

where

$$\frac{1}{Z_r}=\frac{\sqrt{\pi}}{2^{1/2-\gamma}}\cdot\frac{a_f/a_c}{k^{b_f-b_c}}\cdot\frac{m_r{}^{1/2-\gamma}}{\sigma_{ref}}\cdot\left(\frac{m_r}{2(2-\omega)kT_{ref}}\right)\cdot\frac{\Gamma(7/2+\xi_M/2-\gamma)}{\Gamma(7/2+\xi_M/2-\gamma+\chi)},$$
$$\chi=b_f-c_f-1/2+\gamma,$$

https://doi.org/10.4208/cicp.080115.010515s Published online by Cambridge University Press

E_c is the total energy of these three particles and ζ_M is the degree of freedom in internal mode for the third-body particle. The new recombination probability can be obtained by multiplying n_M as $P_{r,new} = P_{r,b} \cdot n_M$. For the DSMC simulation, the mean recombination probability is obtained in the same way as the dissociation method. Then, the rate constant can be determined from Eq. (2.12) as

$$k_b = \frac{\overline{P_{r,new}} \cdot \overline{\sigma g}}{\alpha \cdot n_M}, \qquad \alpha = 2 \text{ for } A = B. \tag{2.14}$$

2.6 Exchange reaction

There are several reactions in air chemistry that exchange the atom under high temperature condition. If a molecule AB reacts with an atom C to form a molecule AC and an atom B, it is a typical exchange reaction which can written as

$$AB + C \to AC + B. \tag{2.15}$$

The derivation of the probability of exchange reaction is the same as the dissociation reaction, which is not repeated here. No matter what kind of chemical reaction is, the Larsen-Borgnakke model [15] is applied to redistribute energies among the translational and internal degrees of freedom.

2.7 Vibrational energy mode

The vibrational energy mode plays a key role of energy redistribution among the translational and internal degrees of freedom in high-temperature air chemistry. The Larsen-Borgnakke method is applied to the vibrational modes through a simple harmonic oscillator with a quantum discrete approach. The vibrational collision (relaxation) number Z_V, which is a function of temperature, can be put into the following form [21] as

$$Z_V = \left(\frac{\theta_d}{T_{coll}}\right)^{\omega} \left[Z_{ref} \left(\frac{T_{z_{ref}}}{\theta_d}\right)^{\omega} \right]^{\left\{ \left[\left(\frac{\theta_d}{T_{coll}}\right)^{1/3} - 1 \right] / \left[\left(\frac{\theta_d}{T_{z_{ref}}}\right)^{1/3} - 1 \right] \right\}}, \tag{2.16}$$

where θ_d is the dissociation characteristic temperature, ω is viscosity index, T_{coll} is the collision temperature and Z_{ref} is the reference vibrational collision number at some reference temperature T_{Zref}, which is usually set as the vibration characteristic temperature θ_v. Z_{ref} can be fitted from the measured data as follows [9, 22]

$$Z_{ref} = \left(\frac{C_1}{T_{z_{ref}}^{\omega}}\right) \exp\left(C_2 T_{z_{ref}}^{-1/3}\right), \tag{2.17}$$

where C_1 and C_2 are both fitted constants. All of the specie properties and constants used in the above equations can be found in Appendix A of [9].

https://doi.org/10.4208/cicp.080115.010515s Published online by Cambridge University Press

3 Results and discussion

In this section, we present several validations of the current implementation for: 1) equilibrium chemical rate coefficients and non-equilibrium transient reservoir chemistry in a single cell, 2) 2D hypersonic cylinder flow and 3) 2D-axisymmetric hypersonic sphere flow. Finally, the PDSC^{++} is applied to simulate the challenging 3D reentry flow of the Apollo Command Module at high altitude to demonstrate its capability. Note that the physics presented in the following will be not thoroughly elaborated since our major purpose is to validate the implementation of chemical reaction module in PDSC^{++}.

3.1 Validation 1: Single-Cell simulations

Equilibrium chemical rate coefficients

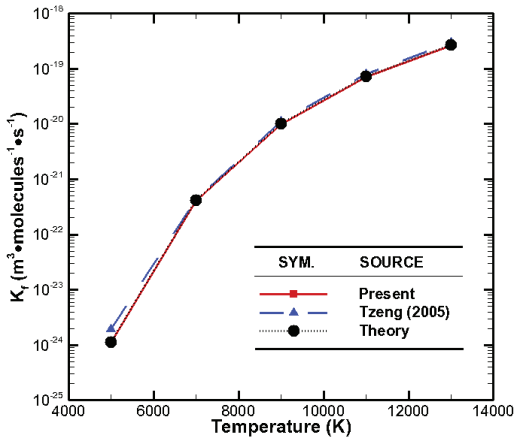
A single three-dimensional cell of side length 1×10^{-5} m was used to calculate the equilibrium chemical rate coefficients (k_f) for three basic types of chemical reaction. The initial number density is assigned as $\rho/\rho_d = 10^5$, where ρ_d is the characteristic density for dissociation, which is a function of temperature [20]. A time step size of 5×10^9s and 50,000 particles were used in each case of simulation. In addition, the rotational collision (relaxation) number was set as 5 and the vibrational collision number was obtained from Eq. (2.16). Note that 50/50% of each species by number is used as the initial conditions for the exchange reaction simulation.

The VHS (variable hard sphere) model [9] was used for collision kinetics, and particles were allowed to move and exchange energy but no particle splitting occurred after reaction. The gas temperature ranges from 3,000 to 13,000 K and only one forward reaction (direction) is considered in different cases. The walls are adiabatic (specular). The reaction probability can be easily calculated as the ratio of the number of collisions that reacts to the total number of collisions in the DSMC simulation. In addition, the rate constant can be readily calculated by using Eq. (2.8) and Eq. (2.14). Fig. 2 shows the simulated rate constants of the typical dissociation, exchange and recombination reactions with different temperatures. The simulated results generally agree very well with the theory and previous simulation data [19]. For the dissociation and exchange reactions, the probabilities increase with increasing temperature because the molecules become more energetic at higher temperature to activate the reactions. On the contrary, the recombination probability decreases with increasing temperature because the atoms become too energetic to form intermediate chemical bonds at higher temperature that is necessary for the recombination reaction to occur.

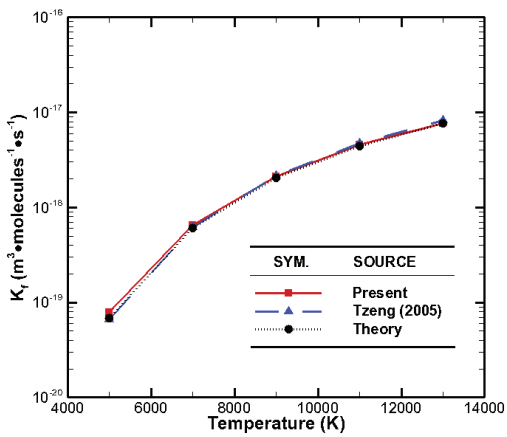
Non-equilibrium time-dependent chemical reactions

For validating the non-equilibrium transient chemical reactions, we have employed an adiabatic gas reservoir considering 5 species (N_2, O_2, NO, N, O) and 34 reaction channels. The results of time-dependent species concentration and temperatures are compared with the analytic solutions obtained from integration of the reaction rate equations.

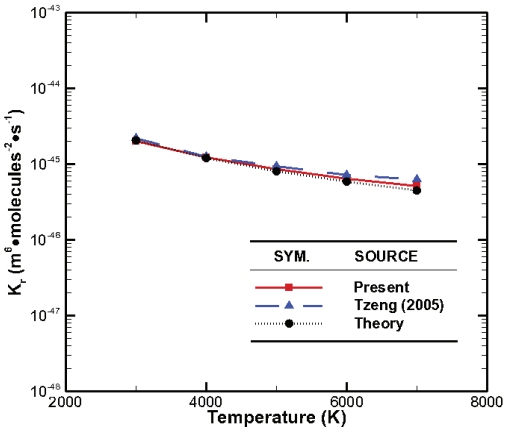
https://doi.org/10.4208/cicp.080115.010515s Published online by Cambridge University Press



(a) $N_2+N_2 \rightarrow N + N + N_2$



(b) $N_2+ O \rightarrow NO + N$



(c) $N + N + N_2 \rightarrow N_2 + N_2$

Figure 2: Equilibrium forward reaction coefficients for typical chemical reactions: (a) dissociation; (b) exchange; (c) recombination.

Unlike previous equilibrium rate simulations, the non-equilibrium chemical transient simulations allow particles to dissociate, exchange, and recombine after reactions. Again, a single cubic cell of side length 1×10^5 m, with six specular surfaces, was used for validation. Following the work of Haas and McDonald [23], a total number of 50,000 particles was used in each simulation, the time step for all test cases was from 0 to 10,000, the rotational collision number was set to 5 and the vibrational collision number was obtained from Eq. (2.16). The molecular collisions were simulated with VHS model. The simulation conditions for non-equilibrium chemical reaction validation were summarized in Table 1. Only the forward reaction was considered during the reaction in cases 1 and 2.

Fig. 3 shows the time-dependent species concentrations and temperature by DSMC

https://doi.org/10.4208/cicp.080115.010515s Published online by Cambridge University Press

Table 1: Simulation conditions for non-equilibrium chemical reaction validation.

Case	T_0, K	P_0, atm	ρ, kg/m3	Concentration	Δt, s
1	20,000	0.063	1.226×10^{-3}	100% O_2	1.520×10^{-9}
2	1,000	5.430	1.226×10^{0}	1% O_2, 99% O	2.414×10^{-12}
3	30,000	1.000	1.172×10^{-2}	21% O_2, 79% N_2	2.321×10^{-10}
4	20,000	1.000	1.757×10^{-2}	21% O_2, 79% N_2	1.421×10^{-10}
5	10,000	1.000	3.515×10^{-2}	21% O_2, 79% N_2	1.005×10^{-10}

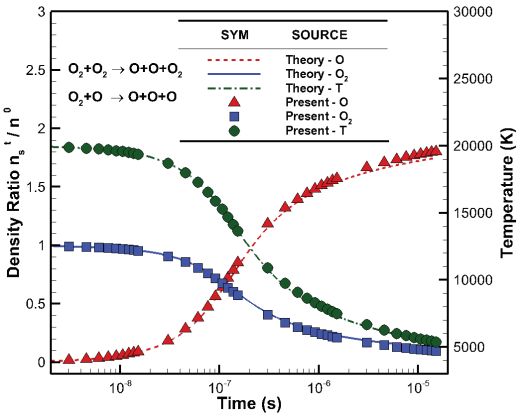


Figure 3: Temporal evolution of species concentrations and temperature of the dissociation of an O_2 reservoir (case 1) in a single-cell DSMC simulation.

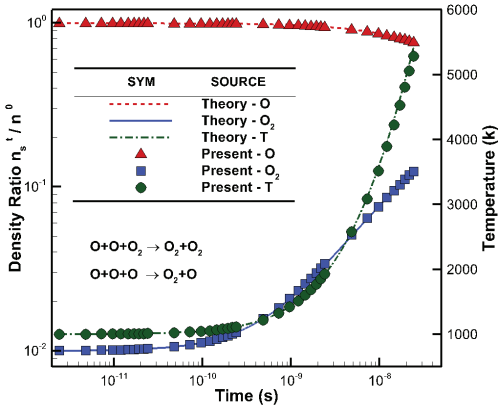


Figure 4: Temporal evolution of species concentrations and temperature of the recombination of an O_2 reservoir (case 2) in a single-cell DSMC simulation.

during the dissociation reaction of a purely diatomic oxygen reservoir at high temperature which relaxes toward equilibrium. The time-dependent species concentrations (n_s^t) is normalized by the initial number density of the species (n_0). As expected for dissoci-

https://doi.org/10.4208/cicp.080115.010515s Published online by Cambridge University Press

ation reaction, which is an endothermic process, removes the thermal energy from the gas and results in a temperature down to approximately 5,500 K from the initial 20,000 K. The DSMC results agree very well with the analytic solution.

Fig. 4 shows the simulated time-dependent oxygen related species concentrations and temperature due to recombination reaction of a monatomic oxygen reservoir. Recombination, which is an exothermic reaction process, heats up the gas and results in a temperature rise to approximately 5,500 K from the initial 1,000 K. In general, the predictions are also in excellent agreement with the analytic solution.

Fig. 5 to Fig. 7 show the temporal evolution of species concentrations and temperature of an air reservoir with initial 21% oxygen and 79% nitrogen at different initial high temperatures of 30,000 K, 20,000 K and 10,000 K, respectively, which is similar to hypersonic flow conditions behind a strong bow shock. The complete set of 34 reactions [19] including 15 dissociation reactions, 15 recombination reactions and 4 exchange reactions as shown in Table 2 is considered. Again, all the DSMC results of the three different cases agree very well with the theoretical solutions.

In brief summary, all the three benchmarking test cases using single-cell DSMC simulations show that the current implementation of chemical reactions considering dissociation, recombination and exchange in the PDSC^{++} are validated with excellent agreement with analytical solutions. Next, we would like to validate the implementation in the PDSC^{++} using some practical flow problems and to compare with previous simulation or experimental data wherever is possible.

3.2 Validation 2: 2D hypersonic cylinder flow

A practical 2D hypersonic cylinder flow was simulated to further validate the implementation of TCE chemistry model in the PDSC^{++}. Free-stream flow conditions included a Mach number of 24.85, a temperature of 187 K and the number density of nitrogen and oxygen is 1.13×10^{-20} and 3.031×10^{-19} particles/m^3, respectively. The cylinder surface was modeled as a fully diffusive wall at a temperature of 1,000K. The rotational and vibrational collision number was set as 5 and 50, respectively. The TCE chemical model with VHS collision mode involved 5 species and 19 reaction channels in the simulation for comparison purpose. The Arrhenius rate coefficients including 15 dissociation reactions and 4 exchange reactions were summarized in Table 1 of Ref. [24]. The simulation consisted of 170,000 unstructured cells, $\sim$ 35 million particles and 100,000 time steps for properties sampling. It took approximately 21 hours of runtime using 96 CPU cores (Intel Xeon X5670, 2.93 GHz, 12M Cache). In addition, TAS and VTS approaches were both applied in the simulation to improve collision quality and reduce the number of iterations required to reach a steady state.

Fig. 8 presents the distribution of merit of collision (MOC) for the DSMC simulation of 2D hypersonic cylinder flow. Merit of collision is a measure of collision quality in a DSMC simulation, defined as the ratio of the mean collision spacing (mcs) to the local mean free path (λ). Generally, the merit of collision (mcs/λ) should be less than unity

https://doi.org/10.4208/cicp.080115.010515s Published online by Cambridge University Press

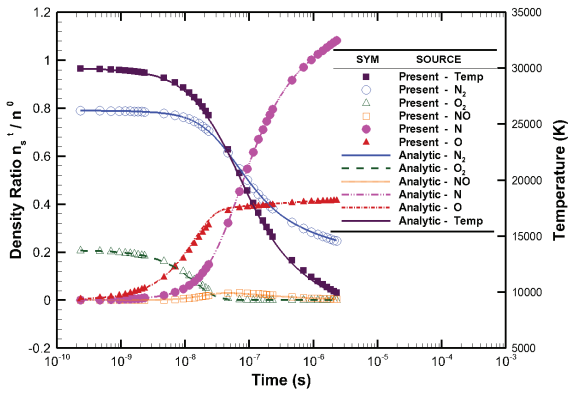


Figure 5: Temporal evolution of species concentrations and temperature of air with an initial temperature of $T_0 = 30{,}000$K (case 3) in a single-cell DSMC simulation.

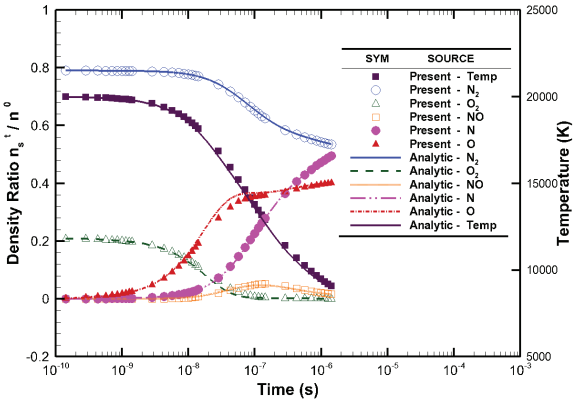


Figure 6: Temporal evolution of species concentrations and temperature of air with initial temperature $T_0 = 20{,}000$K (case 4) in a single-cell DSMC simulation.

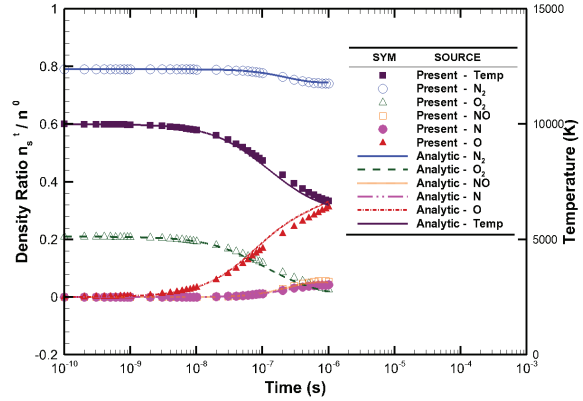


Figure 7: Temporal evolution of species concentrations and temperature of air with initial temperature $T_0 = 10{,}000$K (case 5) in a single-cell DSMC simulation.

https://doi.org/10.4208/cicp.080115.010515s Published online by Cambridge University Press

Table 2: Arrhenius rate variables for the 5- species air model with 34 reactions.

No	Reaction	a	b	Ea(J)	ΔE(J)
1	$N_2+ N_2 \rightarrow N+N+ N_2$	6.17E-09	-1.6	1.56E-18	-1.56E-18
2	$N_2+O_2 \rightarrow N+N+O_2$	6.17E-09	-1.6	1.56E-18	-1.56E-18
3	$O_2+ N_2 \rightarrow O+O+ N_2$	4.58E-11	-1	8.20E-19	-8.20E-19
4	$N_2+NO \rightarrow N+N+NO$	6.17E-09	-1.6	1.56E-18	-1.56E-18
5	$NO+ N_2 \rightarrow N+O+ N_2$	3.83E-13	-0.5	1.04E-18	-1.04E-18
6	$N_2+N \rightarrow N+N+N$	1.85E-08	-1.6	1.56E-18	-1.56E-18
7	$N_2+O \rightarrow N+N+O$	1.85E-08	-1.6	1.56E-18	-1.56E-18
8	$N_2+O \rightarrow NO+N$	5.30E-17	0.1	5.18E-19	-5.18E-19
9	$O2+O_2 \rightarrow O+O+O_2$	4.58E-11	-1	8.20E-19	-8.20E-19
10	$O_2+NO \rightarrow O+O +NO$	4.58E-11	-1	8.20E-19	-8.20E-19
11	$NO +O_2 \rightarrow N+O +O_2$	3.83E-13	-0.5	1.04E-18	-1.04E-18
12	$O_2+N \rightarrow O+O +N$	1.38E-10	-1	8.20E-19	-8.20E-19
13	$O_2+N \rightarrow NO+O$	5.20E-22	1.29	4.97E-20	2.72E-19
14	$O_2+O \rightarrow O+O+O$	1.38E-10	-1	8.20E-19	-8.20E-19
15	$NO +NO \rightarrow N+O+NO$	3.83E-13	-0.5	1.04E-18	-1.04E-18
16	$NO +N \rightarrow N+O +N$	7.66E-13	-0.5	1.04E-18	-1.04E-18
17	$NO+N \rightarrow N_2+O$	2.02E-17	0.1	0	5.18E-19
18	$NO +O \rightarrow N+O+O$	7.66E-13	-0.5	1.04E-18	-1.04E-18
19	$NO+O \rightarrow O_2+N$	3.60E-22	1.29	2.72E-19	-2.72E-19
20	$N+N+ N_2 \rightarrow N_2+ N_2$	5.69E-40	-1.6	0	1.56E-18
21	$N+N+O_2 \rightarrow N_2+O_2$	5.69E-40	-1.6	0	1.56E-18
22	$N+N+NO \rightarrow N_2+NO$	5.69E-40	-1.6	0	1.56E-18
23	$N+N+N \rightarrow N_2+N$	1.71E-39	-1.6	0	1.56E-18
24	$N+N+O \rightarrow N_2+O$	1.71E-39	-1.6	0	1.56E-18
25	$O+O+ N_2 \rightarrow O_2+ N_2$	6.36E-44	-0.5	0	8.20E-19
26	$O+O+O_2 \rightarrow O2+O_2$	6.36E-44	-0.5	0	8.20E-19
27	$O+O+NO \rightarrow O_2+NO$	6.36E-44	-0.5	0	8.20E-19
28	$O+O+N \rightarrow O_2+N$	1.91E-43	-0.5	0	8.20E-19
29	$O+O+O \rightarrow O_2+O$	1.91E-43	-0.5	0	8.20E-19
30	$N+O+ N_2 \rightarrow NO+ N_2$	1.58E-43	-0.5	0	1.04E-18
31	$N+O+O_2 \rightarrow NO+O_2$	1.58E-43	-0.5	0	1.04E-18
32	$N+O+NO \rightarrow NO+NO$	1.58E-43	-0.5	0	1.04E-18
33	$N+O+N \rightarrow NO+N$	3.18E-43	-0.5	0	1.04E-18
34	$N+O+O \rightarrow NO+O$	3.18E-43	-0.5	0	1.04E-18

for the DSMC simulation to be considered accurate, as advocated in [25, 26]. The results show that the MOC is generally much smaller than unity and the maximal MOC occurs near the stagnation point and the value is about 0.5.

https://doi.org/10.4208/cicp.080115.010515s Published online by Cambridge University Press

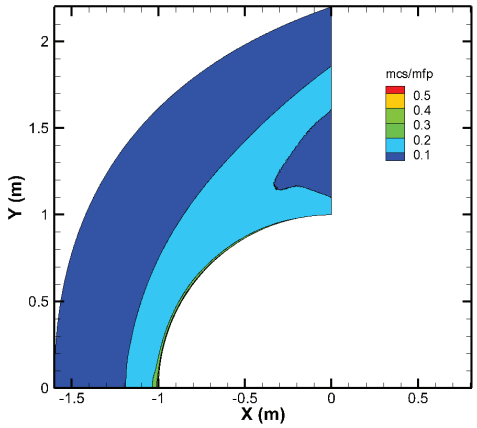


Figure 8: Distribution of merit of collision of 2D hypersonic cylinder flow ($M_\infty = 24.85$, $T_\infty = 187$ K).

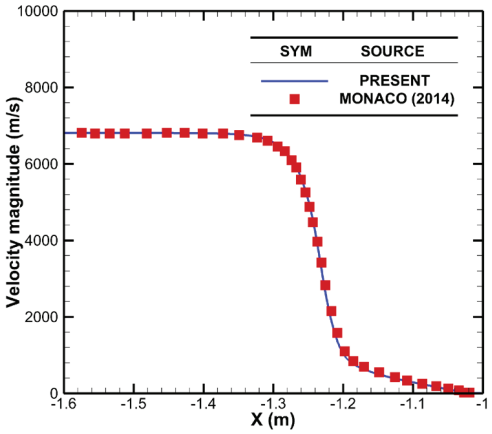


Figure 9: Velocity profile along the stagnation centerline using PDSC^{++} (line) and MONACO (symbol) of 2D hypersonic cylinder flow ($M_\infty = 24.85$, $T_\infty = 187$ K).

Figs. 9 to 11 show the comparison of distributions of velocity magnitude, number densities and temperatures, respectively, along the stagnation streamline with the simulation data by MONACO code [24]. All the results show that the current DSMC simulation results agree very well with those of Ref. [24]. Fig. 9 shows that the velocity profiles predicted by both codes along the stagnation streamline are in good agreement, and the shock lies approximately 20-30 cm from the cylinder stagnation point. Fig. 11 shows that there is a considerable amount of thermal non-equilibrium within the shock wave as indicated by the fact that the rotational and vibrational temperature are well below the translational temperature. All of the temperature distributions are in close agreement with those predicted by MONACO [24] and the maximal translational, rotational and vibrational temperature along the stagnation streamline is approximately 20,000 K, 14,000 K and 9,000 K, respectively.

https://doi.org/10.4208/cicp.080115.010515s Published online by Cambridge University Press

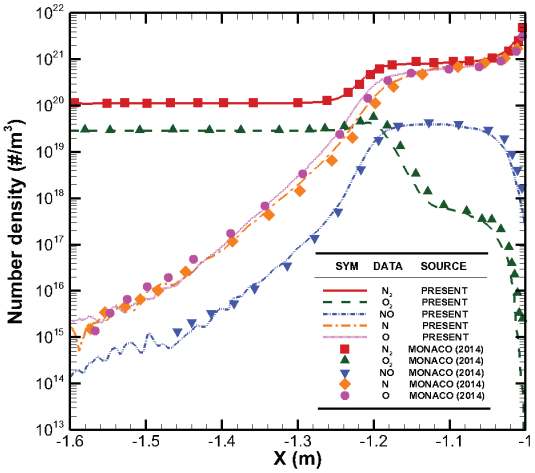


Figure 10: Number density profiles along the stagnation centerline using PDSC^{++} (line) and MONACO (symbol) of 2D hypersonic cylinder flow ($M_\infty = 24.85$, $T_\infty = 187$ K).

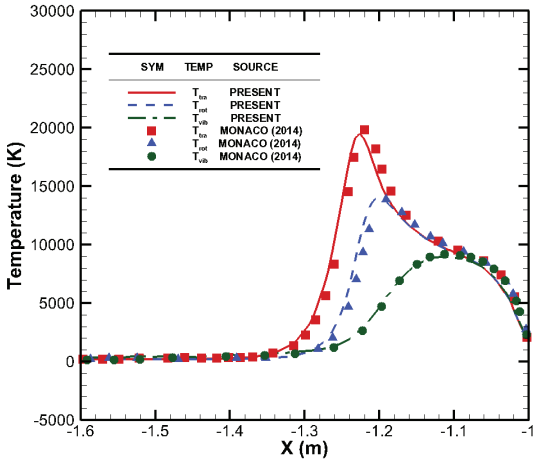


Figure 11: Temperature profiles along the stagnation centerline using PDSC^{++} (line) and MONACO (symbol) of 2D hypersonic cylinder flow ($M_\infty = 24.85$, $T_\infty = 187$ K).

Figs. 12-14 show the comparison of the simulated distributions of translational, rotational and vibrational temperatures, respectively, with those of Ref. [24]. The results show that the agreement is in general excellent for most of the flow field except some subtle differences in certain regions. This may be caused by the different number of cells, distribution of cells and number of particles, which were not clearly stated in Ref. [24], as compared to the present study. Fig. 15 and Fig. 16 show the comparison of distributions of Mach number and NO number density, respectively, with those by MONACO [24]. It is found that the PDSC^{++} predicts a thinner distribution of species layer across the shock wave region as compared to that of MONACO. Note that the computational domains of

https://doi.org/10.4208/cicp.080115.010515s Published online by Cambridge University Press

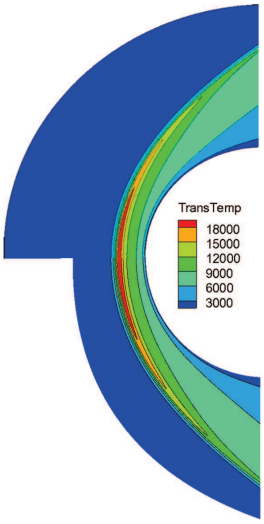


Figure 12: Distribution of translational temperature predicted using PDSC^{++} (lower half) and MONACO (upper half) of 2D hypersonic cylinder flow ($M_\infty = 24.85$, $T_\infty = 187$ K).

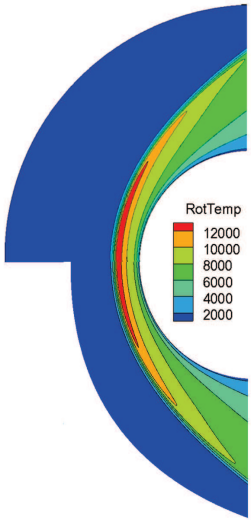


Figure 13: Distribution of rotational temperature predicted using PDSC^{++} (lower half) and MONACO (upper half) of 2D hypersonic cylinder flow ($M_\infty = 24.85$, $T_\infty = 187$ K).

the upper part in Figs. 12-16 are adopted directly from Ref. [24]. Nonetheless, the general flow features appear to be very similar as predicted by both codes. Finally, Fig. 17 shows distribution of the surface properties of pressure and heat flux. The peak value of the surface pressure and heat flux is approximately 300 Pa and 65 kW/m^2, respectively. The distributions of surface properties are also in good agreement with those by MONACO.

3.3 Validation 3: 2D-axisymmetric hypersonic sphere flow

Hypersonic flow past a sphere was used for the validation of 2D-axisymmetric PDSC^{++}. Test conditions are the same as those in Dogra *et al.* [27]. The free-stream conditions corresponding to the Earth's atmosphere at an altitude of 90 km included a Mach number of 27.2, a density of 3.43×10^{-6} kg/m^3, a velocity of 7,500 m/s and a temperature of 188 K. In addition, ambient air included oxygen molecule, nitrogen molecule and oxygen atom in molar fraction are 0.209, 0.788 and 0.004, respectively. The sphere wall temperature is fixed as 350 K with a fully diffuse surface. The corresponding free-stream Knudsen number (Kn) and Reynolds number (Re) (based on the diameter of the sphere, 1.6 meter) are 0.01 and 3,243 respectively. We simulated this 3D case using 2D-axisymmetric PDSC^{++} by taking advantage of flow symmetry. Radial weighting technique [9] in combination with VTS and TAS are employed to reduce the number of simulation particles without sacrificing the solution accuracy. The cell number and particle number were about 50,000 and 2,000,000, respectively.

We have employed rotational relaxation number and vibrational relaxation number

https://doi.org/10.4208/cicp.080115.010515s Published online by Cambridge University Press

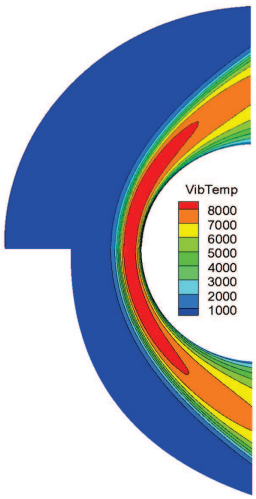


Figure 14: Distribution of vibrational temperature predicted using PDSC^{++} (lower half) and MONACO (upher half) of 2D hypersonic cylinder flow ($M_\infty = 24.85$, $T_\infty = 187$ K).

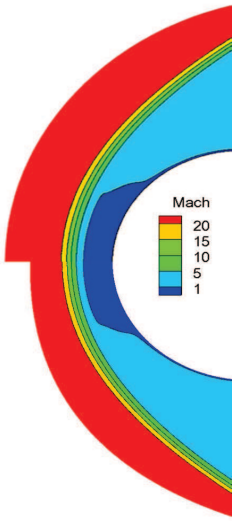


Figure 15: Distribution of Mach number predicted using PDSC^{++} (lower half) and MONACO (upper half) of 2D hypersonic cylinder flow ($M_\infty = 24.85$, $T_\infty = 187$ K).

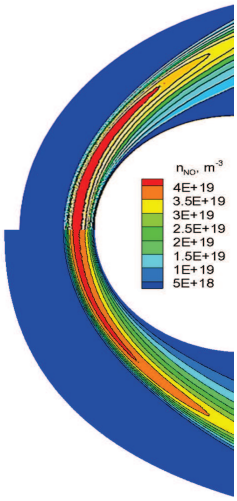


Figure 16: Distribution of NO number density predicted using PDSC^{++} (lower half) and MONACO (upper half) of 2D hypersonic cylinder flow ($M_\infty = 24.85$, $T_\infty = 187$ K).

as 5 and 50 respectively, which might be different from those used in Ref. [27] since these values were not described clearly. The TCE chemical model with VHS collision mode included 5 species and 34 reaction channels. The Arrhenius rate coefficients included 15 dissociation reactions, 15 recombination reactions and 4 exchange reactions [27].

https://doi.org/10.4208/cicp.080115.010515s Published online by Cambridge University Press

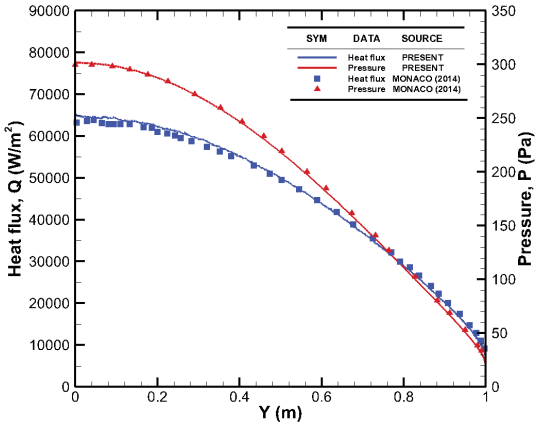


Figure 17: Pressure and heat flux distributions along the surfaces using PDSC^{++} (line) and MONACO (symbol) of 2D hypersonic cylinder flow ($M_\infty = 24.85$, $T_\infty = 187$ K).

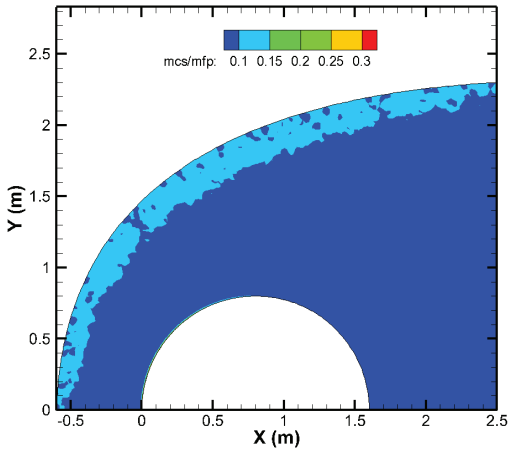


Figure 18: Distribution of merit of collision of 2D-axisymmetric hypersonic sphere flow ($M_\infty = 27.2$, $T_\infty = 188$ K).

Fig. 18 shows the resulting distribution of merit of collision of the DSMC simulation, in which maximal MOC is smaller than 0.3 and MOCs in most of the flow region is well below 0.1. This represents that the DSMC simulation had a very good collision quality.

Fig. 19 presents the molar fractions of all species, including N_2, O_2, NO, N and O, along the stagnation centerline. The amounts of NO, N and O increase when the flow approaches the bow shock region due to the chemical reactions caused by the strong bow shock, which mostly are from dissociation and exchange reactions. Fig. 20 shows the distribution of translational, rotational and vibrational temperatures, in which there is significant thermal non-equilibrium near the shock region. Appreciable discrepancy of

https://doi.org/10.4208/cicp.080115.010515s Published online by Cambridge University Press

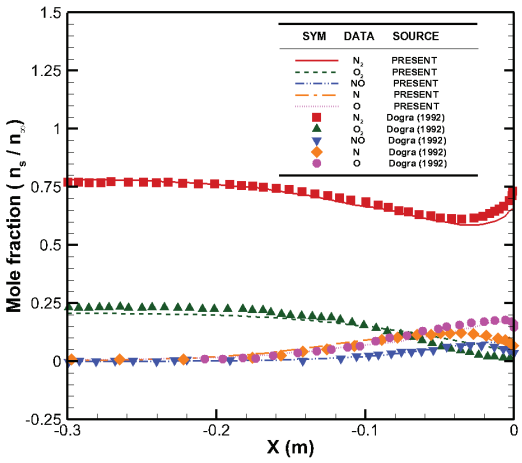


Figure 19: Number density profiles along the stagnation centerline of axisymmetric hypersonic sphere flow ($M_\infty = 27.2$, $T_\infty = 188$ K).

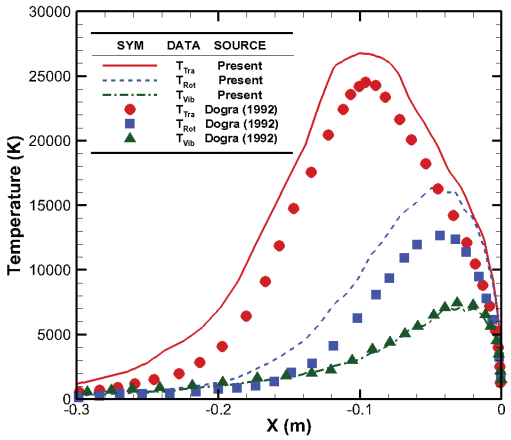


Figure 20: Temperature profiles along the stagnation centerline of axisymmetric hypersonic sphere flow ($M_\infty = 27.2$, $T_\infty = 188$ K).

translational and rotational temperatures is found between the present results and those of Ref. [27] probably because different energy redistribution model and recombination mode were used. Although these distributions do not exactly agree with previous simulation data, the present results have the similar trend in general which are both reasonable.

Figs. 21-23 show some typical distributions of flow properties (normalized density, normalized overall temperature and Mach number) around the sphere, in which the normalized properties are based on the free-stream conditions. There is a very strong bow shock standing in the front of the sphere and a highly rarefied wake region exists behind the sphere. Fig. 24 shows the comparison of surface properties between the present

https://doi.org/10.4208/cicp.080115.010515s Published online by Cambridge University Press

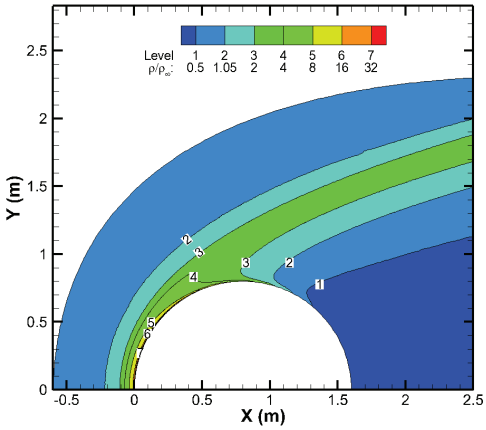


Figure 21: Distribution of normalized density of axisymmetric hypersonic sphere flow ($M_\infty=27.2$, $T_\infty=188$ K).

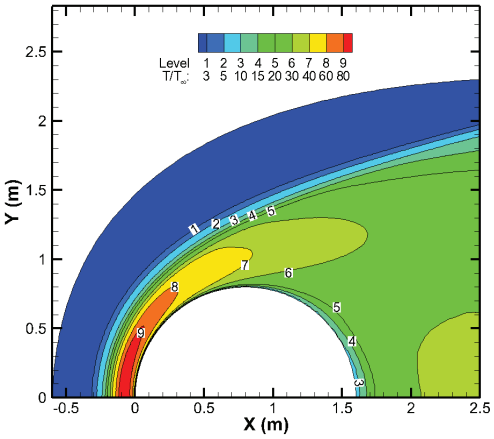


Figure 22: Distribution of normalized temperature of axisymmetric hypersonic sphere flow ($M_\infty=27.2$, $T_\infty=188$ K).

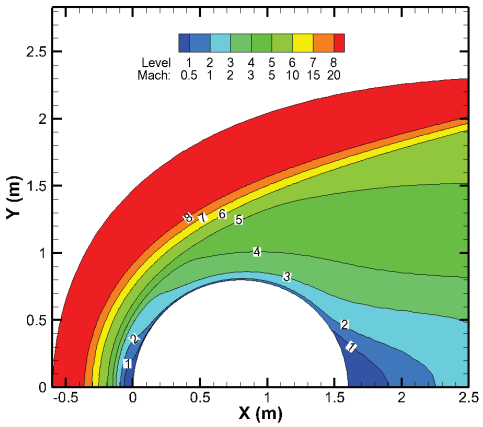


Figure 23: Distribution of Mach number of axisymmetric hypersonic sphere flow ($M_\infty=27.2$, $T_\infty=188$ K).

https://doi.org/10.4208/cicp.080115.010515s Published online by Cambridge University Press

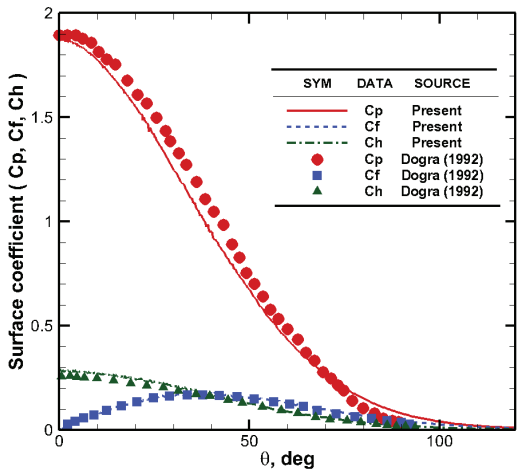


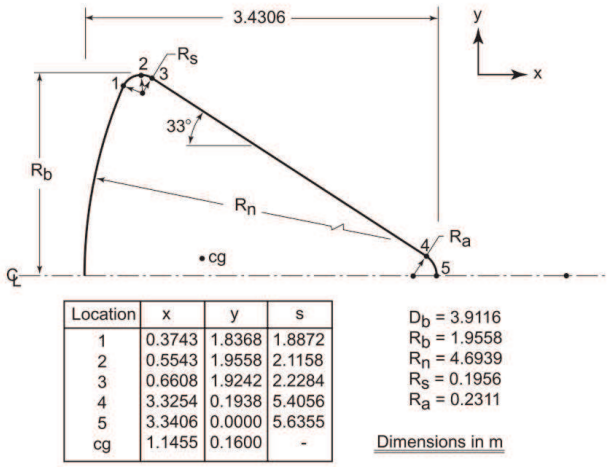
Figure 24: Surface coefficients as a function of circumferential angle (θ) along the sphere surface ($M_\infty = 27.2$, $T_\infty = 188$ K).

and previous work [27], including pressure, skin-friction and heat transfer coefficients, as a function of circumferential angle (θ), measured clockwise from the stagnation point, along the sphere surface. The pressure and heat transfer coefficients decrease with increasing θ with a maximal value of 1.91 and 0.28 at stagnation point $\theta = 0^\circ$ respectively. However, the skin-friction coefficient increases first then decreases along the sphere surface with a maximal value of 0.19 at $\theta = 38^\circ$. In addition, skin-friction coefficients are generally one order of magnitude smaller than pressure coefficients as expected. Generally, the simulated results agree very well with previous work [27].

3.4 Application: Reentry flow of Apollo command module

In this section, we would like to present the application of the PDSC^{++} for simulating a realistic hypersonic flow past a three-dimensional Apollo 6 Command Module [28], which is shown in Fig. 25 that was simulated by using DS3V [9]. In the simulation, only half of the domain is simulated by taking advantage of the geometrical symmetry to save the computational cost. Nomenclature used for aerodynamic coefficients of the body (axial and normal) and velocity (drag and lift) oriented coordinates are shown in Fig. 26. Related free-stream conditions at an altitude of 105 km are described next in turn. The number densities of free-stream gases, including nitrogen, oxygen and oxygen atom, were 3.993×10^{18}, 8.054×10^{17} and 2.992^{17}, respectively. In addition, the velocity with an incidence angle of -25° and temperature were 9,600 m/s and 208 K, respectively, which the corresponding Mach number is 33.2. A fully diffusive wall was employed and the wall temperature was fixed at 1,029 K. The rotational and vibrational collision numbers were fixed as 5 and 50 respectively. The TCE chemical model with VHS collision mode involved 5 species and 34 reaction channels in the simulation, which the corresponding

https://doi.org/10.4208/cicp.080115.010515s Published online by Cambridge University Press



Location	x	y	s
1	0.3743	1.8368	1.8872
2	0.5543	1.9558	2.1158
3	0.6608	1.9242	2.2284
4	3.3254	0.1938	5.4056
5	3.3406	0.0000	5.6355
cg	1.1455	0.1600	-

D_b = 3.9116
R_b = 1.9558
R_n = 4.6939
R_s = 0.1956
R_a = 0.2311

Dimensions in m

Figure 25: Schematic diagram of axisymmetric geometry of the Apollo 6 Command Module [28].

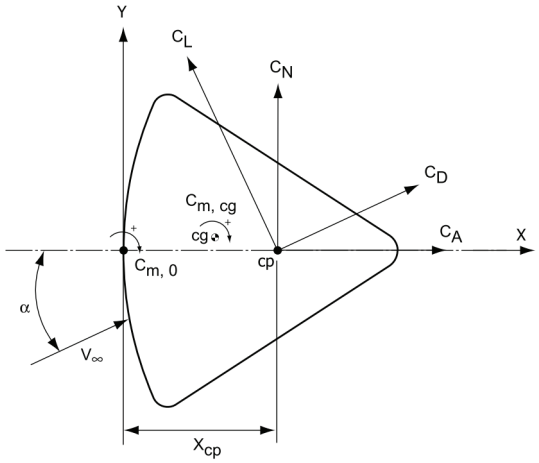


Figure 26: Nomenclature for aerodynamic forces of Apollo 6 Command Module [28].

Arrhenius rate coefficients could be found in Ref. [28]. Free-stream Knudsen number (Kn) was 0.081. Number of cells and number of particles of this simulation were approximately 600,000 and 20,000,000 respectively. Fig. 27 shows the distribution of MOC for the DSMC simulation, in which the maximal value is ∼2 at the surface, which is slightly high. However, it should be acceptable considering the very high computational cost for 3D simulation, should the maximal MOC value be strictly limited to be smaller than unity.

Figs. 28-30 show the distributions of normalized density, normalized temperature and Mach number, based on the free-stream conditions. Figs. 31-35 present the distributions of mole fractions of N_2, O_2, NO, N and O, respectively, on the symmetrical plane of the

https://doi.org/10.4208/cicp.080115.010515s Published online by Cambridge University Press

Table 3: Comparison of aerodynamic coefficients of Apollo 6 Command Module ($M_\infty = 33.2$, $T_\infty = 208$ K).

	C_A	C_N	C_D	C_L	L/D
Present	1.459	-0.343	1.467	0.306	0.208
Moss (2006)	1.529	-0.374	1.544	0.307	0.199
Difference	4.58%	8.29%	5%	0.3%	4.52%

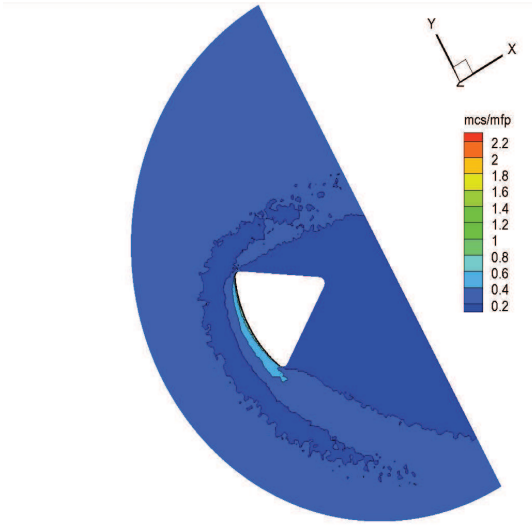


Figure 27: Sliced distribution of merit of collision of hypersonic flow past an Apollo 6 Command Module ($M_\infty = 33.2$, $T_\infty = 208$ K).

Apollo 6 Command Module. The results show that a strong bow shock appears in front of the Command Module, while a highly rarefied region is formed behind. Abundant amounts of NO and N species in front of the spacecraft are also produced due to the high temperature caused by the strong bow shock. Table 3 summarizes the simulated aerodynamic coefficients along with those predicted in Ref. [28], which shows that they agree very well within 5% in general.

4 Conclusion

We have implemented the DSMC chemistry models based on the TCE approach successfully within the PDSC^{++} code for the use in hypersonic rarefied gas flows. Several benchmark test cases, including singe-cell simulations, 2D hypersonic cylinder flow and 2D-axisymmetric sphere flow, validate the proper implementation of chemical modules. Finally, a 3-D challenging hypersonic Apollo re-entry flow is simulated and compared with previous published simulation data using DS3V [28]. All of these validations and demonstration show that the TCE chemical-reaction module has been successfully im-

https://doi.org/10.4208/cicp.080115.010515s Published online by Cambridge University Press

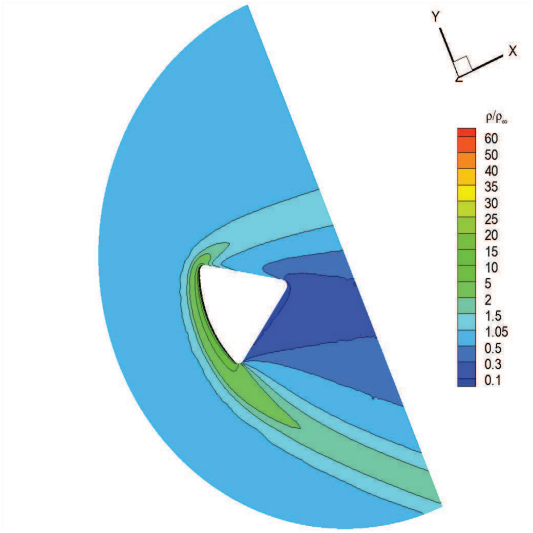


Figure 28: Sliced distribution of normalized density of hypersonic flow past an Apollo 6 Command Module ($M_\infty = 33.2$, $T_\infty = 208$ K).

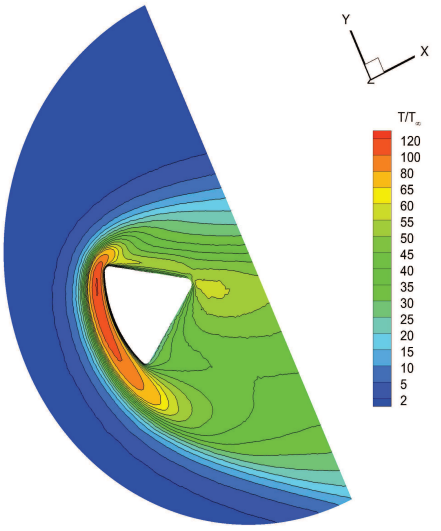


Figure 29: Sliced distribution of normalized temperature of hypersonic flow past an Apollo 6 Command Module ($M_\infty = 33.2$, $T_\infty = 208$ K).

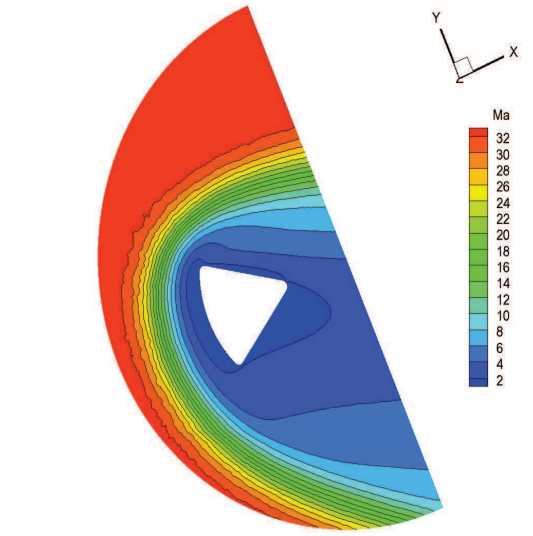


Figure 30: Sliced distribution of Mach number of hypersonic flow past an Apollo 6 Command Module ($M_\infty = 33.2$, $T_\infty = 208$ K).

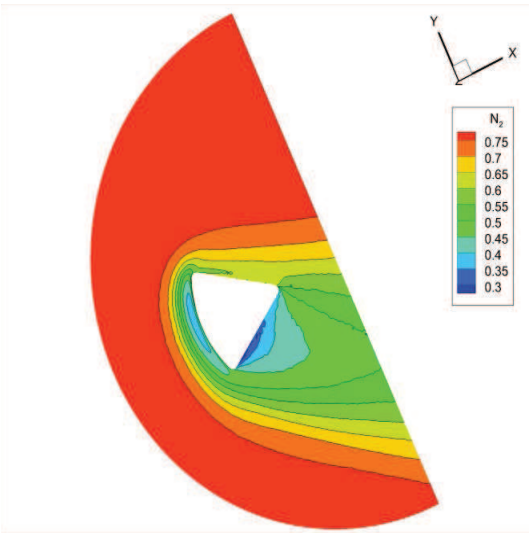


Figure 31: Sliced distribution of N_2 mole fraction of hypersonic flow past an Apollo 6 Command Module ($M_\infty = 33.2$, $T_\infty = 208$ K).

plemented in the present PDSC^{++}. Simulations of EXPERT based on planned flight envelope [5] using the PDSC^{++} is currently in progress and will be reported elsewhere in the very near future.

https://doi.org/10.4208/cicp.080115.010515s Published online by Cambridge University Press

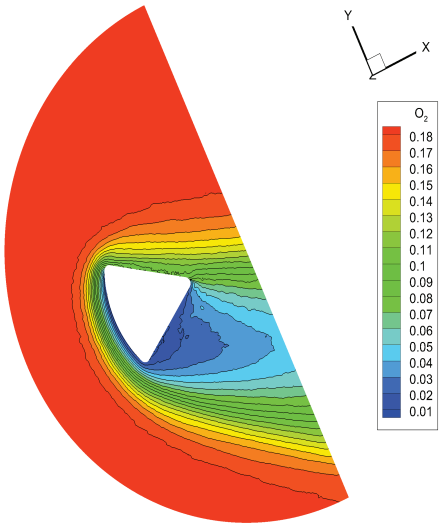


Figure 32: Sliced distribution of O_2 mole fraction of hypersonic flow past an Apollo 6 Command Module ($M_\infty = 33.2$, $T_\infty = 208$ K).

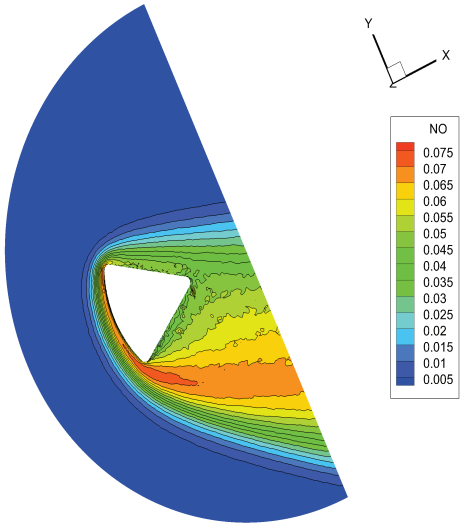


Figure 33: Sliced distribution of NO mole fraction of hypersonic flow past an Apollo 6 Command Module ($M_\infty = 33.2$, $T_\infty = 208$ K).

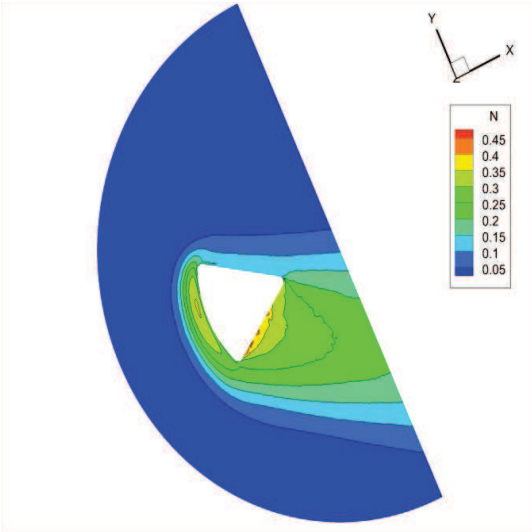


Figure 34: Sliced distribution of N mole fraction of hypersonic flow past an Apollo 6 Command Module ($M_\infty = 33.2$, $T_\infty = 208$ K).

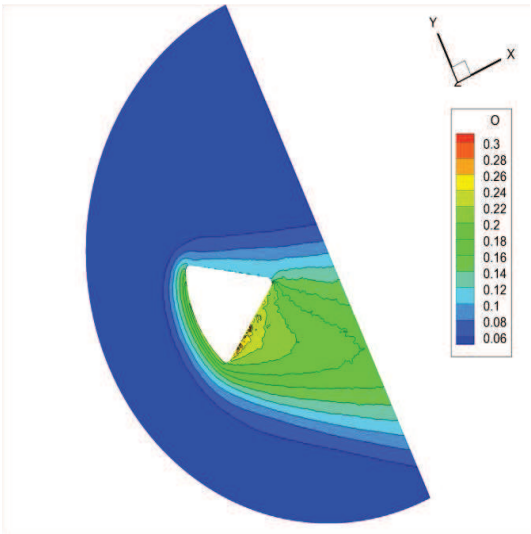


Figure 35: Sliced distribution of O mole fraction of hypersonic flow past an Apollo 6 Command Module ($M_\infty = 33.2$, $T_\infty = 208$ K).

Acknowledgments

We would like to express our appreciation for the computing resources provided by the National Center for High-Performance Computing of Taiwan. The authors would also like to acknowledge the support obtained from the National Science Council (NSC) of

https://doi.org/10.4208/cicp.080115.010515s Published online by Cambridge University Press

Taiwan through research grants including NSC 102-2627-E-009-001 and MOST103-2923-E-009-004-MY3.

References

[1] T. McIntyre, W. Beck and J. Lacey, The high enthalpy shock tunnel in Gottingen, AIAA Pap. No. 39-42, 1992.
[2] G. Eitelberg, First result of calibration and use of the HEG, AIAA Pap. No. 94-2525, 1994.
[3] M. Holden, Recent advances in hypersonic test facilities and experimental research, AIAA Pap. No. 93-5005, 1993.
[4] H. Weihs, J. Longo and J. Turner, The Sharp Edge Flight Experiment SHEFEX II, a mission overview and status, AIAA Paper 2008-2542, 2008.
[5] J. Muylaert, L. Walpot, H. Ottens and F. Cipollini, Aerothermodynamic Reentry Flight Experiment EXPERT, RTO-EN-AVT-130-13, 2007.
[6] J.-S. Wu and Y.-Y. Lian, Parallel three-dimensional direct simulation Monte Carlo method and its applications, Computers & Fluids, 32 (2003), 1133-1160.
[7] J.-S. Wu, K.-C. Tseng, and F.-Y. Wu, Parallel three-dimensional DSMC method using mesh refinement and variable time-step scheme, Journal of Computer Physics Communications, 162 (2004), 166-187.
[8] C.-C. Su, K.-C. Tseng, H. M. Cave, J.-S. Wu, Y.-Y. Lian, T.-C. Kuo and M. C. Jermy, Implementation of a transient adaptive sub-cell module for the parallel-DSMC code using unstructured grids, Computers & Fluids, 39 (2010), 1136-1145.
[9] G. A. Bird, Molecular Gas Dynamics and the Direct Simulation of Gas Flows, Clarendon Press, Oxford, 1994.
[10] W. Wagner, A convergence proof for bird's direct simulation Monte Carlo method for the Boltzmann equation, Journal of Statistical Physics, 66 (1992), 1011-1044.
[11] G. J. LeBeau and F. E. Lumpkin Iii, Application highlights of the DSMC Analysis Code (DAC) software for simulating rarefied flows, Computer Methods in Applied Mechanics and Engineering, 191(6) (2001), 595-609.
[12] I. D. Boyd, Vectorization of a Monte Carlo simulation scheme for nonequilibrium gas dynamics, Journal of Computational Physics, 96(2) (1991), 411-427.
[13] M. Ivanov, G. Markelov, S. Taylor, J. Watts, Parallel DSMC strategies for 3D computations, Proceedings of the Parallel CFD, 96 (1997), 485-492.
[14] I. D. Boyd, Analysis of vibration-dissociation-recombination processes behind strong shock waves of nitrogen, Physics of Fluids A: Fluid Dynamics (1989-1993), 4(1) (1992), 178-185.
[15] C. Borgnakke and P. S. Larsen, Statistical collision model for Monte Carlo simulation of polyatomic gas mixture, Journal of Computational Physics, 18 (1975), 405-420.
[16] J.-S. Wu and K.-C. Tseng, Parallel DSMC method using dynamic domain decomposition, International Journal for Numerical Methods in Engineering, 63 (2005), 37-76.
[17] K. C. Kannenberg and I. D. Boyd, Strategies for efficient particle resolution in the direct simulation Monte Carlo method, Journal of Computational Physics, 157(2) (2000), 727-745.
[18] G. A. Bird, The DS2V/3V program suite for DSMC calculations, in Rarefied Gas Dynamics: Proceedings of the 24th International Symposium on Rarefied Gas Dynamics, edited by M. Capitelli, AIP Conference Proceedings, 762, Melville, NY (2005), 541-546.
[19] K.-C. Tseng, J.-S. Wu and I. D. Boyd, Simulations of re-entry vehicles by using DSMC with chemical-reaction module, 14th AIAA/AHI Space Planes and Hypersonic Systems and Technologies Conference, 2006.

https://doi.org/10.4208/cicp.080115.010515s Published online by Cambridge University Press

[20] W. G. Vincenti and C. H. Kruger, Introduction to Physical Gas Dynamics, Wiley, New York, 1965.
[21] G. A. Bird, A comparison of collision energy-based and temperature-based procedures in DSMC, AIP Conference Proceedings, 1084(1) (2008), 245-250.
[22] R. C. Millikan and D. R. White, Systematics of vibrational relaxation, Journal of Chemical Physics, 39(12) (1963), 3209-3213.
[23] B. L. Haas and J. D. McDonald, Validation of chemistry models employed in a particle simulation method, Journal of Thermophysics and Heat Transfer, 7(1) (1993), 595-609.
[24] J. S. Thomas, W. Craig, K. B. Matthew, C. P. Rodrigo, F. Erin, D. B. Iain, M. R. Jason and E. B. Richard, Open source DSMC chemistry modelling for hypersonic flows, AIAA Journal. ISSN 0001-1452 (Submitted) http://strathprints.strath.ac.uk/46619/.
[25] G. A. Bird, Sophisticated versus simple DSMC, in Proceedings of the 25th International Symposium on Rarefied Gas Dynamics (RGD25), 2006.
[26] M. A. Gallis, J. R. Torczynski, D. J. Rader, G. A. Bird, Accuracy and convergence of a new DSMC algorithm, 40th AIAA Thermophysics Conference, AIAA, Vol. 2913, 2008.
[27] V. K. Dogra, R. G. Wilmoth and J. N. Moss, Aerothermodynamics of a 1.6-meter-diameter sphere in hypersonic rarefied flow, AIAA Journal, 30(7) (1992), 1789-1794.
[28] J. Moss, C. Glass and F. Greene, DSMC simulations of Apollo capsule aerodynamics for hypersonic rarefied conditions, AIAA Paper 2006-3577, 2006.

https://doi.org/10.4208/cicp.080115.010515s Published online by Cambridge University Press